

## A frequency multiplexed near-infrared topography system for imaging functional activation in the brain

N. L. Everdell,<sup>a)</sup> A. P. Gibson, and I. D. C. Tullis

*Department of Medical Physics & Bioengineering, University College London, Malet Place Engineering Building, Gower Street, London WC1E 6BT, United Kingdom*

T. Vaithianathan

*Centre for Advance Manufacturing Research, University of South Australia, Mawson Lakes Boulevard, Mawson Lakes, SA 5095, Australia*

J. C. Hebden and D. T. Delpy

*Department of Medical Physics and Bioengineering, University College London, Malet Place Engineering Building, Gower Street, London WC1E 6BT, United Kingdom*

(Received 26 March 2005; accepted 26 July 2005; published online 2 September 2005)

We have developed a novel near-infrared optical topography system that can acquire images of functional activation in the human brain at 10 frames per second using 32 detectors. The image acquisition rate is inversely proportional to the number of detectors, so the maximum acquisition rate using four detectors is 80 Hz. 16 laser diode sources (8 at 785 and 8 at 850 nm) are illuminated simultaneously, and each of 8 avalanche photodiode detectors records light from several sources at the same time. The contribution from each source is demultiplexed in software using fast Fourier transforms. This allows for a more flexible, smaller, and less complex system than is achievable using traditional hardware demodulation techniques, such as lock-in amplifiers. The system will eventually incorporate a total of 64 sources and 32 detectors, enabling the entire adult cortex to be imaged. The system is designed to be as flexible as possible, and to be applicable to a wide variety of experimental and clinical needs. To this end, it can operate in two distinct modes: As a frequency multiplexed system and as a time multiplexed system. We describe phantom and in vivo investigations that have been undertaken using the new instrument in its frequency multiplexed operating mode. © 2005 American Institute of Physics. [DOI: [10.1063/1.2038567](https://doi.org/10.1063/1.2038567)]

### I. INTRODUCTION

Diagnostic methods are being developed which exploit the high transmittance of tissue at near-infrared (NIR) wavelengths. In particular, the different specific absorption characteristics of oxyhaemoglobin (HbO<sub>2</sub>) and deoxyhaemoglobin (HHb) enable blood content and oxygenation to be derived. NIR topography enables spatially resolved changes in activation to be recorded from an array of sources and detectors placed against the scalp. This provides a two-dimensional map of functional activity within the cortex.<sup>1</sup>

The first topography systems were demonstrated more than 10 years ago, and subsequent years have seen a steady development of both equipment and applications. The first systems to be available commercially were developed by Hitachi Medical Systems. Their ETG 100 system<sup>2</sup> has 20 laser diode sources (10 at each of 2 wavelengths of 780 and 830 nm) and 8 avalanche photodiode detectors (APD). Each laser diode is intensity modulated at a different frequency. The output from each detector is fed into a set of lock-in amplifiers which can discriminate between the different frequencies in the detected signal. This method, known as frequency multiplexing (or sometimes frequency encoding), allows all of the sources to be illuminated simultaneously, so

that an image can be obtained more quickly. This system has been used in a wide variety of investigations.<sup>3–10</sup> A more recent system developed by Hitachi, the ETG 7000, can image the entire adult cortex with 40 pairs of laser diodes and 40 APD detectors. Other similar systems have also been employed to image the cortex of both newborn babies and adults. Hintz *et al.*<sup>11</sup> used a system with 18 laser diode sources and 16 photodiode detectors for a passive motor activation study in newborn babies. The CW4 system used by Franceschini *et al.*<sup>12</sup> has 16 laser diode sources and 16 avalanche photodiode detectors. It is also a frequency multiplexed system, but uses infinite impulse response filters to separate source signals rather than Fourier transforms. Their system has been employed to study motor cortex activation in adults.

Danen *et al.*<sup>13</sup> have developed a system with 12 sources and 4 detectors that records both the amplitude and the phase of the modulated signal (commonly known as a frequency domain system). Their system was used to image a shunt inside the skull of a patient with hydrocephalus. Franceschini *et al.*<sup>14</sup> have employed a similar system, based on 16 intensity modulated sources and two photomultiplier tube detectors. This system has also been used for a motor cortex activation study in adults.

<sup>a)</sup>Electronic mail: everdell@medphys.ucl.ac.uk

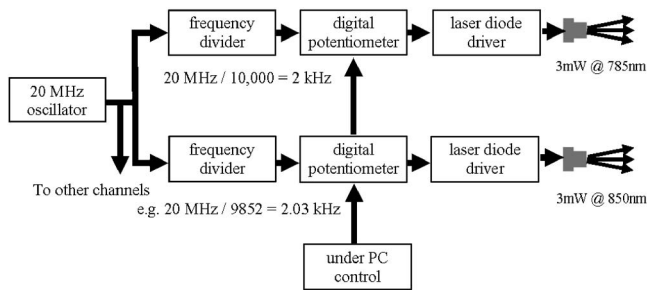


FIG. 1. Block diagram of laser sources.

## II. THE UNIVERSITY COLLEGE LONDON OPTICAL TOPOGRAPHY SYSTEM

### A. Description of system

At University College London (UCL), we have developed a novel approach to optical topography which involves using software to demultiplex multiple source signals which are modulated at different frequencies in parallel. This allows great flexibility in the positioning of sources and detectors. A range of different optical fiber arrays can be used with only minor changes being needed to the software. The system currently employs 16 laser diode sources (8 at 785 nm and 8 at 850 nm) and 8 avalanche photodiode detectors, but will eventually have 64 sources and 32 detectors. With this specification, a device based on hardware demultiplexing would require over 100 lock-in amplifier circuits, increasing size, cost, and complexity.

The choice of source wavelengths has been a subject of much discussion. The “NIR window” for tissue imaging is between 650 and 850 nm. Often sources are chosen to have wavelengths either side of the isobestic point of haemoglobin, at 800 nm. This is the wavelength at which the specific extinction coefficients of HbO<sub>2</sub> and HHb are equal. A typical pair of wavelengths might be 780 and 830 nm. However, more recently, it has been shown<sup>8,15,16</sup> that using a lower wavelength between 660 and 760 nm rather than 780 nm provides better differentiation between HHb and HbO<sub>2</sub>. In light of these findings, the system will in the future employ a lower wavelength source of 760 nm instead of 785 nm.

A block diagram of the laser sources is shown in Fig. 1, and the detection system is outlined in Fig. 2. All of the multiplexing frequencies are derived from the same 20 MHz quartz oscillator, which prevents any relative drift in frequency between different sources. The oscillator signal is fed into a frequency divider which reduces the frequency into the kilohertz range. A digital potentiometer then enables the amplitude of the resulting square wave to be adjusted to the required level. Finally, the square wave modulates the laser diode via a driver circuit. Currently there are 16 laser diode sources (8 lasers at 785 nm and 8 at 850 nm), driven by

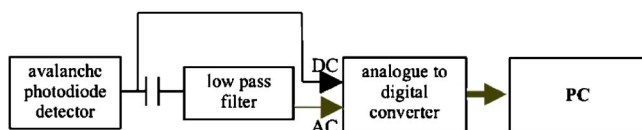


FIG. 2. Block diagram of detector.

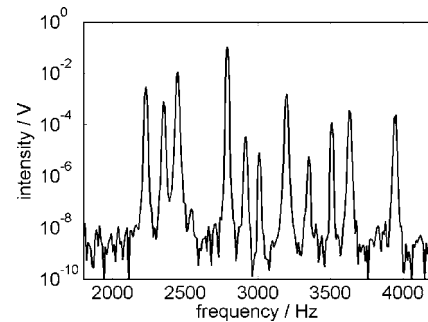


FIG. 3. An example of an FFT of the data from one detector.

frequencies ranging from 2 kHz to 4 kHz. The mean power emitted by each laser diode is approximately 2 mW. The frequencies are kept within one octave to prevent interference from harmonics.

Our system currently employs 8 Hamamatsu C5460-01 APDs, each with a 3 mm diameter collecting area and a measurement bandwidth of approximately 100 kHz. The signal from these is ac coupled into an eight-pole low-pass filter that has a 3 dB point at 4 kHz. This allows for 64 dB of roll off before the Nyquist frequency of 10 kHz, so aliasing is prevented. The output from the antialiasing filter is fed into an analog to digital converter which samples each channel at 20 kHz. The data acquisition hardware currently being used is a 14-bit 400 kilosample/s PCI board (United Electronic Industries PD2-MF-16-400/14H). This would allow up to 20 detector channels to be sampled at 20 kilosamples/s. The signal can be sampled directly from the APD (both dc and ac components) or from the output of the low-pass filter (just an ac component). Control, data acquisition and data processing software has been written in C and runs within the National Instruments LabWindows/CVI environment.

The raw data from all the detector channels are stored in a circular memory buffer, which can hold several seconds worth of data. Subsequent processing is performed serially on data taken from this buffer, rather than directly from the data acquisition card. In this way, data can be continuously acquired as well as continuously processed. The subsequent processing [detrending, fast Fourier transforms (FFTs), etc.] is quick enough to keep up with the incoming data stream, so no data are lost.

The data are detrended using a Hanning window on a 2048 point sample. A FFT is subsequently performed in software to separate the different source signals. A typical spectrum obtained from a detector is shown in Fig. 3. Each peak corresponds to a nearby source from which the detector is receiving a signal. There are 11 distinct peaks in the spectrum because this particular detector can see 11 nearby sources.

Each frequency bin of the FFT is 10 Hz wide. The signal from each source will not be contained entirely within a bin of such small bandwidth. Therefore, the amplitudes from five bins on each side of the center frequency, as well as the center frequency itself, are summed together to obtain the light intensity received from each source. The intensity information for each source-detector pair is displayed in real time. Changes in absorption, oxy-, and deoxyhaemoglobin

concentration are calculated from the raw data using a separate MATLAB program. The time taken for these calculations is small compared to the data acquisition cycle time (0.1 s) so it will be straightforward to display this information in real time. From the intensity data, a spatial map of optical absorption of the tissue under interrogation can be built up as described in Sec. II B.

The raw data from the detectors are not stored, as the data transfer rate and the resultant file sizes would be prohibitive. Instead, the received intensity for each source-detector pair is written to a text file as a double precision floating point number. For the current system of 16 sources and 8 detectors, this results in a file of size 7.5 megabytes for a data acquisition time of 10 min.

The system is designed to be able to produce an image every tenth of a second using the information from 32 detectors. There is an inverse relationship between the number of active detectors and the frame rate that can be achieved. Thus, a system with just 16 active detectors can operate at a rate of 20 frames/s. Using fewer detectors with a faster acquisition rate would allow the system to investigate fast neuronal signals.<sup>17</sup> These signals are thought to originate from the changes in refractive index that occur as a result of neuronal depolarization. The time scale of these changes, of the order of 10–100 ms, is much smaller than that of the haemodynamic response, which occurs over a few seconds. We expect to be able to image these changes by acquiring an image every 25 ms using eight detectors.

In addition to this frequency multiplexed scheme, the system can also operate in a time multiplexed scheme, which involves illuminating individual laser sources in turn for a short period. Although this has the disadvantage of reducing the image acquisition rate, the overall signal to noise ratio of the data is increased as there is less background light contributing shot noise to the measurement. As for the frequency multiplexed mode of operation, a subset of sources can be selected so that a smaller area of the cortex can be interrogated, and the rate of acquisition of images increased.

Sources and detectors are both coupled to the tissue under investigation via simple multimode poly(methyl methacrylate) (PMMA) optical fibers, of 1 mm diameter. These fibers can be held in arrays of various different designs. One such array consists of a thermoplastic shell that is molded to the shape of the part of the body under investigation (see Sec. III B). The interior surface of the shell is lined with soft light-absorbing foam. The signal to noise ratio across 3 cm of tissue equivalent phantom material at maximum optical power has been found to be approximately 600:1 (56 dB) for an integration time of 0.1 s. This compares favorably with our measured figure for the Hitachi ETG 100 system of 500:1 (54 dB). Currently, the data acquisition card encodes the received optical signals to a depth of 14 bits, although this will eventually be increased to 16 bits.

## B. Reconstruction algorithm

The array being used for experiments is comprised of multiple source-detector separations, so three-dimensional (3D) tomographic image reconstruction is particularly suitable. Image reconstruction has been shown<sup>18</sup> to provide bet-

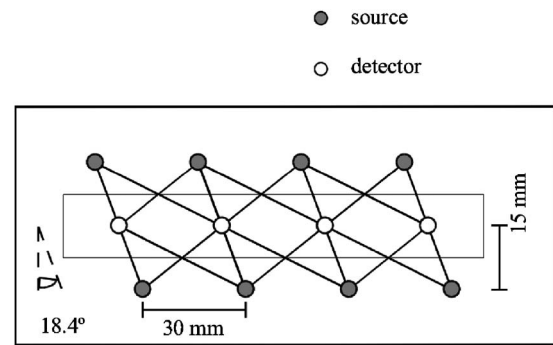


FIG. 4. Geometry of optical fiber array.

ter overall image quality than the more usual two-dimensional mapping technique. Accordingly, 3D images were reconstructed using the Rytov approximation.<sup>19</sup> Measured changes in  $\log(\text{amplitude})$ ,  $\mathbf{y}$ , were assumed to be related to changes in the optical absorption,  $\mathbf{x}$ , by the matrix equation  $\mathbf{y}=\mathbf{A}\mathbf{x}$ , where  $\mathbf{A}$  is the Jacobian or sensitivity matrix. Here,  $\mathbf{A}$  was calculated by solving the diffusion equation using the finite element method applied to a finite element mesh of tetrahedra with quadratic interpolation functions, which was generated using Netgen.<sup>20</sup> Images were generated by Tikhonov regularisation of the Moore–Penrose generalized inverse  $\mathbf{x}=\mathbf{A}^T(\mathbf{A}\mathbf{A}^T+\lambda\mathbf{I})^{-1}\mathbf{y}$ , where the regularization parameter  $\lambda$  was set to 1% of the largest singular value of  $\mathbf{A}\mathbf{A}^T$ . The computationally intensive calculation and inversion of the sensitivity matrix is performed offline. Images can then be generated by a matrix multiplication in real time.

## III. EXPERIMENTAL WORK

### A. Dynamic liquid phantom

For a preliminary evaluation of the system and the reconstruction algorithm, an array was devised that employs 16 sources and 4 detectors, as shown in Fig. 4. This array has potentially many distinct source-detector separations. The maximum separation over which a signal can be detected through tissue has been found to be approximately 40 mm. For this array, the useful separations are 15.8 mm, 25 mm, and 38.1 mm. For the two detectors nearest the center of the array, a signal can be obtained from the six nearest sources. In total, there are 20 source-detector pairs with separations less than 40 mm.

The array is shown attached to a phantom in Fig. 5. The phantom consists of a tank of scattering fluid with one wall made from a 5 mm thick epoxy resin slab. The slab has optical properties of absorption coefficient ( $\mu_a$ )=0.01 mm<sup>-1</sup>, reduced scattering coefficient ( $\mu'_s$ )=1 mm<sup>-1</sup>, and refractive index 1.56. The absorption coefficient is wavelength dependent, but not significantly. It remains within 10% of its value at 800 nm over the range 780 to 850 nm. The other walls are made from infrared absorbing plastic. The tank is filled with an aqueous solution of intralipid<sup>21</sup> and absorbing dye, with optical properties of  $\mu_a$ =0.007 mm<sup>-1</sup> and  $\mu'_s$ =0.8 mm<sup>-1</sup>. The absorber here shows a similar wavelength dependence to that used in the resin slab. A stepper motor is mounted on the lid, which enables a small target to be rotated within the

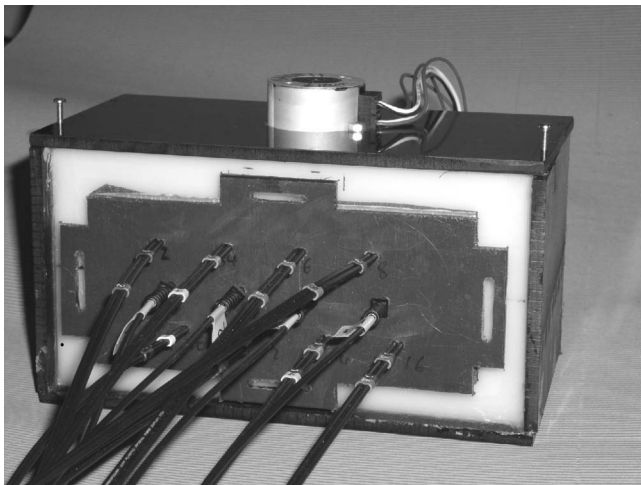


FIG. 5. Liquid Phantom—the optical fiber array is attached to the front face.

liquid, suspended on a short length of rigid wire. The target consists of an epoxy resin cylinder, 10 mm in length, and 10 mm in diameter, with the same scattering properties as the surrounding liquid, but ten times the absorption. The motor enables the target to be rotated in a plane perpendicular to the face of the phantom in a circle of diameter 60 mm, and at a speed of up to 1 rev/s. Intensity data were collected from the entire set of sources and detectors at a rate of 10 Hz. The closest approach the target made to the plane of the sources and detectors was 15 mm. Values of log intensity at the wavelength of 780 nm were used to reconstruct images of the moving target using the algorithm described in Sec. II B.

Each column of Fig. 6 shows three slices through the 3D image of absorption taken parallel to the plane of the sources and detectors at depths of 5, 10, and 15 mm, respectively. From left to right, Fig. 6 shows the target cylinder entering and crossing the field of view. The maximum change in absorption is  $0.04 \text{ mm}^{-1}$  and occurs at a depth of 5 mm. This image was reconstructed from a single set of image data with no temporal block averaging.

The target appears nearer to the surface in the image than its actual position, but its depth can be seen to change as it moves from left to right across the field of view, indicating that there is qualitative depth discrimination. The depth discrimination can be expected to be limited due to the topographic array geometry. Boas *et al.*<sup>18</sup> demonstrated that an arrangement of sources and detectors with multiple separations, such as used here, provides improved spatial discrimi-

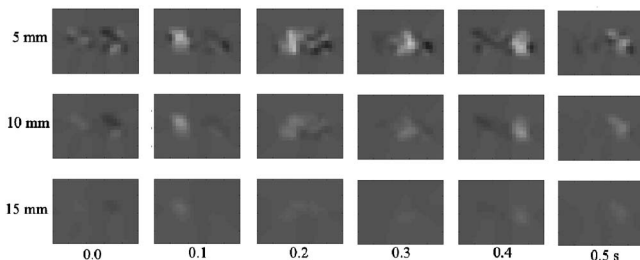


FIG. 6. 3D reconstruction of liquid phantom experiment. The columns show the image at intervals of 0.1 s and the rows show slices at increasing depths through the image—5 mm, 10 mm, and 15 mm.

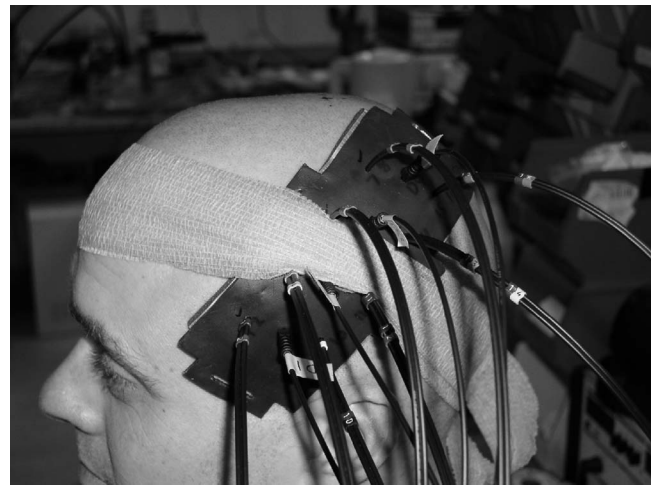


FIG. 7. A thermoplastic optical fiber array for adult motor cortex experiments.

nation in a plane parallel to that of the source and detectors; here, we show a similar improvement with depth.

## B. Adult motor cortex experiments

Experiments on adult volunteers have been performed in order to determine the ability of the system to detect functional activation of the motor cortex. The thermoplastic base of the array was moulded to fit the shape of each individual subject's head (Fig. 7). The array was designed to image the motor cortex. The inner rectangle (125 mm by 18 mm) in Fig. 4 represents an estimate of the size and shape of the adult motor cortex, based on anatomical information.

The array was positioned over the estimated position of the left motor cortex as shown in Fig. 7. The subject was asked to perform a finger opposition task with his right hand for 30 s followed by 40 s of rest. This cycle was repeated eight times so that the data could be block averaged together. The intensity data showed a considerably reduced signal to noise ratio when compared to the data obtained from a tissue equivalent phantom. For the smallest source-detector separation of 15.8 mm, it was 29 dB. For the 25 mm separation it was 20 dB, and for the largest separation of 38.1 mm it was 11 dB. This is likely to be caused at least in part by reduced coupling between the optical fibers and the head.

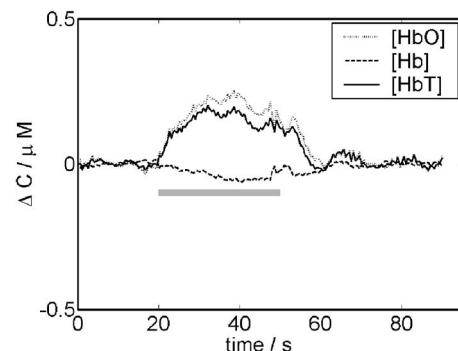


FIG. 8. Data from one source-detector pair of separation 15.8 mm. The graph shows changes in oxy-, deoxy-, and total haemoglobin over a period of 90 s. The horizontal grey bar shows the period of finger tapping.

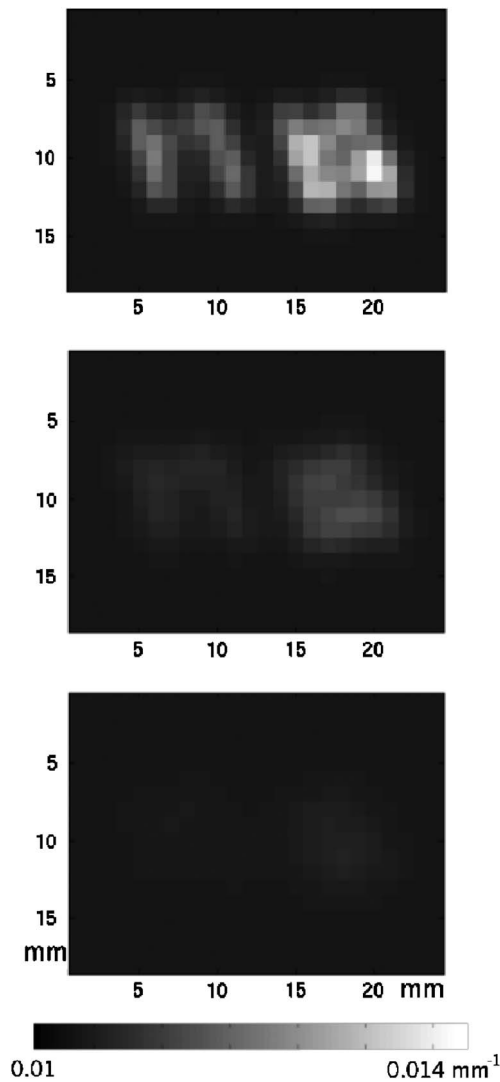


FIG. 9. A topographic image showing activation of the motor cortex. This image predominantly shows an increase in absorption of 40% at 850 nm due to an increase in blood volume in the motor cortex.

The intensity data from the two different wavelengths was used to calculate changes in absorption coefficient ( $\Delta\mu_a$ ) using the differential pathlength factor (DPF) method.<sup>22</sup> The DPF itself was assumed to be 5. We used these values of  $\Delta\mu_a$  at 785 nm and 850 nm to estimate changes in the concentrations of oxyhaemoglobin and deoxyhaemoglobin. Published values for extinction coefficients of the two chromophores were used for this calculation.<sup>23</sup>

A typical functional response curve showing these changes for one source-detector pair is shown in Fig. 8. This data are derived from block averaging the eight trials described previously. In this graph, the horizontal grey bar represents the period of time when the subject was performing the motor task. An increase in the concentration of oxyhaemoglobin of approximately  $2.5 \mu\text{M}$  can be clearly seen. There is a corresponding but smaller decrease in the concentration of deoxyhaemoglobin of approximately  $0.05 \mu\text{M}$ . The change in total haemoglobin, which is simply the sum of the other two traces, is shown as well. The size of these

changes compares reasonably well with other published data on motor cortex evoked responses.<sup>12</sup>

An absorption image reconstructed from similarly block averaged intensity data acquired at 850 nm is shown in Fig. 9. The figure again shows three slices through the 3D image of absorption taken parallel to the plane of the sources and detectors at depths of 5, 10, and 15 mm, respectively. For this reconstruction, it is assumed that the sources and detectors all lie in the same plane. The absorption increase is higher on the right half of the image than in the left half. This corresponds to a larger haemodynamic response in the superior half of the motor cortex (see Fig. 7).

The change is largest at a depth of 5 mm. The adult motor cortex lies at a depth of approximately 15 mm, so the depth has not been correctly localized due to the limitations of a topographic geometry. However, the results from the phantom experiment described earlier suggest that the novel arrangement of sources and detectors with multiple separation may provide some depth discrimination.

#### ACKNOWLEDGMENT

The authors would like to acknowledge the contribution made by Professor S. Arridge and Dr. M. Schweiger in providing algorithms to calculate the sensitivity matrix used in this work. System development was funded by the Wellcome Trust.

- <sup>1</sup>H. Obrig and A. Villringer, *J. Cereb. Blood Flow Metab.* **23**, 1 (2003).
- <sup>2</sup>Y. Yamashita, A. Maki, and H. Koizumi, *J. Biomed. Opt.* **4**, 414 (1999).
- <sup>3</sup>A. Maki, Y. Yamashita, Y. Ito, E. Watanabe, Y. Mayanagi, and H. Koizumi, *Med. Phys.* **22**, 1997 (1995).
- <sup>4</sup>E. Watanabe, A. Maki, F. Kawaguchi, K. Takashiro, Y. Yamashita, H. Koizumi, and Y. Mayanagi, *Neurosci. Lett.* **256**, 49 (1998).
- <sup>5</sup>E. Watanabe, A. Maki, F. Kawaguchi, Y. Yamashita, H. Koizumi, and Y. Mayanagi, *J. Epilepsy* **11**, 335 (1998).
- <sup>6</sup>E. Watanabe, Y. Nagahori, and Y. Mayanagi, *Epilepsia* **43**, 50 (2002).
- <sup>7</sup>K. Takahashi, S. Ogata, Y. Atsumi, R. Yamamoto, S. Shiotsuka, A. Maki, Y. Yamashita, T. Yamamoto, H. Koizumi, H. Hirasawa, and T. Imai, *J. Biomed. Opt.* **5**, 93 (2000).
- <sup>8</sup>Y. Yamashita, A. Maki, and H. Koizumi, *Med. Phys.* **28**, 1108 (2001).
- <sup>9</sup>H. Koizumi, T. Yamamoto, A. Maki, Y. Yamashita, H. Sato, H. Kawaguchi, and N. Ichikawa, *Appl. Opt.* **42**, 3054 (2003).
- <sup>10</sup>A. Obata, K. Morimoto, H. Sato, A. Maki, and H. Koizumi, *Psychiatry Res.: Neuroimag.* **123**, 145 (2003).
- <sup>11</sup>S. R. Hintz, D. A. Benaron, A. M. Siegal, A. Zourabian, D. K. Stevenson, and D. A. Boas, *J. Perinat. Med.* **29**, 335 (2001).
- <sup>12</sup>M. A. Franceschini, S. Fantini, J. H. Thompson, J. P. Culver, and D. A. Boas, *Psychophysiology* **40**, 548 (2003).
- <sup>13</sup>R. M. Danen, Y. Wang, X. D. Li, W. S. Thayer, and A. G. Yodh, *Photochem. Photobiol.* **67**, 33 (1998).
- <sup>14</sup>M. A. Franceschini, V. Toronov, M. E. Filiaci, E. Gratton, and S. Fantini, *Opt. Express* **6**, 49 (2000).
- <sup>15</sup>G. Strangman, M. A. Franceschini, and D. A. Boas, *Neuroimage* **18**, 865 (2003).
- <sup>16</sup>K. Uludag, J. Steinbrink, A. Villringer, and H. Obrig, *Neuroimage* **22**, 583 (2004).
- <sup>17</sup>M. A. Franceschini and D. A. Boas, *Neuroimage* **21**, 372 (2004).
- <sup>18</sup>D. A. Boas, A. M. Dale, and M. A. Franceschini, *Neuroimage* **23**, S275 (2004).
- <sup>19</sup>S. R. Arridge, *Inverse Probl.* **15**, 41 (1999).
- <sup>20</sup>J. Schöberl, *Comput. Visual. Sci.* **1**, 41 (1997).
- <sup>21</sup>H. J. Van Staveren, C. J. M. Moes, J. van Marle, S. A. Prah, and M. J. C. van Gemert, *Appl. Opt.* **30**, 4507 (1991).
- <sup>22</sup>D. T. Delpy, M. Cope, P. van der Zee, S. Arridge, S. Wray, and J. Wyatt, *Phys. Med. Biol.* **33**, 1433 (1988).
- <sup>23</sup>M. Cope, Ph.D thesis University of London, 1991.